Tailoring accelerating beams in phase space

Yuanhui Wen,[1] Yujie Chen,[1,*] Yanfeng Zhang,[1] Hui Chen,[1] and Siyuan Yu[1,2]

[1]*State Key Laboratory of Optoelectronic Materials and Technologies, School of Electronics and Information Technology,
Sun Yat-sen University, Guangzhou 510275, China*
[2]*Photonics Group, Merchant Venturers School of Engineering, University of Bristol, Bristol BS8 1UB, United Kingdom*

An appropriate wave-front design will enable light fields that propagate along arbitrary trajectories, thus forming accelerating beams in free space. Previous strategies for designing such accelerating beams rely mainly on caustic methods, which start from diffraction integrals and deal only with two-dimensional fields. Here we introduce an alternate perspective to construct accelerating beams in phase space by designing the corresponding Wigner distribution function (WDF). We find that such a WDF-based method is capable of providing both the initial field distribution and the angular spectrum in need by projecting the WDF into the real space and the Fourier space, respectively. Moreover, this approach applies to the construction of both two- and three-dimensional fields, greatly generalizing previous caustic methods. It may therefore open a new route for construction of highly tailored accelerating beams and facilitate applications ranging from particle manipulation and trapping to optical routing as well as material processing.

I. INTRODUCTION

A wave front contains the essential information on light including the phase, amplitude, and polarization, which can be engineered by various optical elements ranging from conventionally bulky to newly planar optical components [1–6]. An appropriate wave-front design can lead to light fields capable of propagating along curved trajectories in free space, namely, accelerating beams. This seemingly counterintuitive discovery was revealed in 2007; a light field with an Airy distribution propagates along a parabolic trajectory [7,8]. This peculiar property makes accelerating beams attractive for a variety of potential applications, such as micromanipulation [9,10], micromachining [11], imaging [12,13], optical routing [14], light bullets [15,16], laser-assisted guiding of electric discharge [17], and plasma generation [18]. Moreover, due to the similar form of wave equations, the fundamental research on optical accelerating beams can be readily generalized to acoustic waves [19], electron waves [20], and plasmonic waves [21–23], with a broad and important influence beyond optics.

For the applications to be flexible enough, accelerating beams propagating along various trajectories are required. Thus how to associate a desired propagating trajectory with an appropriate wave front remains a crucial problem. One strategy is to keep on finding other rare analytical solutions of the wave equation, while a more efficient way is based on the caustic method, which associates the desired trajectory with an optical caustic, the envelope of a family of light rays [24–26]. This method was first implemented in real space [27,28] and successfully realized arbitrary convex propagating trajectories for two-dimensional (2D) light fields, while the caustic method in Fourier space was also proposed subsequently [29–31]. Therefore, for one predesigned trajectory, accelerating beams can be constructed by caustic methods either in real space or in Fourier space, but the relationship between them is not clear

yet. Moreover, the present caustic methods mainly focus on 2D fields, and the usual extension to three-dimensional (3D) fields relies on the separability of the two transverse directions (x,y) or rotation of the established 2D fields, which is still a 2D situation essentially. Hence, to our knowledge, the real 3D fields have not yet been investigated with the present caustic methods.

To associate field distributions in real space and Fourier space, one may come up with the Wigner distribution function (WDF), an alternative representation which was introduced originally in quantum mechanics and has become a powerful tool in optics. The physical meaning of the WDF in optics can be approximately interpreted as the intensity of a light ray with a specific position and direction. Particularly, the WDF has been exploited to study the propagation of Airy beams [32,33], which provides an intuitive picture to explain the novel characteristics of these accelerating beams. Since the propagation properties of accelerating beams are related to the WDF, a question naturally arises: Is it possible to construct accelerating beams simply by engineering the WDF?

In this paper, we introduce a new perspective to describe and construct accelerating beams. In contrast to previous caustic methods starting from the diffraction integrals in real space or Fourier space, we begin with the design of the WDF in phase space [34,35]. This new perspective is capable of revealing the relationship between the aforementioned caustic methods in real space and those in Fourier space in the 2D case. Additionally, in the 3D case, beyond the analytical scope of previous caustic methods, our approach is still applicable and explicitly points out a new class of 3D accelerating beams, which includes the familiar helicon waves [36–38].

II. THEORECTICAL ANALYSIS

The essential idea of our theoretical analysis is more generic and applicable to both 2D and 3D fields. For the sake of clarity, here we present the study in the 2D case under the paraxial condition, where the transverse variation is only along the X axis (independent of the Y axis) and the propagating direction
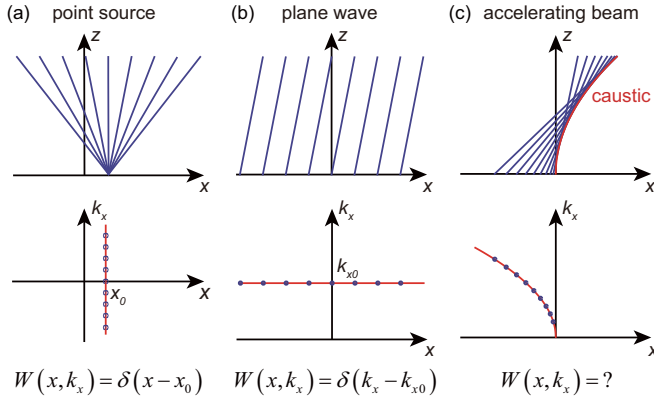
*chenyj69@mail.sysu.edu.cn

FIG. 1. Schematic showing the light-ray picture and the corresponding form of the WDF in phase space for (a) a point source, (b) a plane wave, and (c) an accelerating beam.

is along the Z axis. Particularly, the coordinate for the initial plane $(X,Y,0)$ is denoted (x,y) for simplicity. As mentioned, we begin with the phase-space design of the WDF in the initial plane, which is defined as

$$W(x,k_x) = \int E(x + x'/2)E^*(x - x'/2)e^{-ik_x x'}dx'$$
$$= \int A(k_x + k'_x/2)A^*(k_x - k'_x/2)e^{ik'_x x}dk'_x, \quad (1)$$

where $E(x)$ is the initial field distribution, while $A(k_x)$ is the corresponding angular spectrum with k_x the spatial frequency, and an asterisk denotes throughout complex conjugation. The physical meaning of the WDF in optics can be approximately interpreted as the intensity of a light ray passing through position x in direction (or at spatial frequency) k_x, but it may take a negative value due to the interference of waves [34,35].

In general, the WDF of a light field in phase space does not have an analytical form, except for some specific cases, such as a point source and a plane wave as shown in Figs. 1(a) and 1(b). The WDFs of a point source located at position x_0 and a plane wave at spatial frequency k_{x0} are $\delta(x - x_0)$ and $\delta(k_x - k_{x0})$, respectively. The expressions show a clear physical picture that a point source contains the light rays emanating from the same initial point x_0 in all directions k_x, while a plane wave contains the light rays emanating from all the initial points x in the same direction k_{x0}. When it comes to the accelerating beam represented by its caustic trajectory, it is natural to ask what its WDF looks like in phase space and what is the relationship between the caustic trajectory and the WDF.

Note that it is impossible to work out the exact WDF if given only the caustic trajectory, but we may construct a WDF with inspiration from the WDF forms of a point source or a plane wave. Figure 1(c) shows that for a given caustic trajectory $X = f(Z)$, each ray tangent to the caustic has a specific initial position $x = f(Z) - Zf'(Z) \triangleq F_1(Z)$ and direction $k_x = kf'(Z) \triangleq F_2(Z)$ (here k is the wave number in free space), corresponding to a point (x,k_x) located in phase space. Thus a WDF can be constructed by integrating all the

above points and expressed mathematically as

$$W(x,k_x) = \int_0^{Z_{\max}} \delta(x - F_1(Z))\delta(k_x - F_2(Z))dZ. \quad (2)$$

Based on this constructed WDF and its properties, we can directly obtain the initial field distribution $E(x) = \rho(x)e^{i\varphi(x)}$ as

$$\rho^2(x) = \int W(x,k_x)dk_x, \quad \varphi'(x) = \frac{\int k_x W(x,k_x)dk_x}{\int W(x,k_x)dk_x} \quad (3)$$

and the angular spectrum $A(k_x) = P(k_x)e^{i\Phi(k_x)}$ as

$$P^2(k_x) = \int W(x,k_x)dx, \quad \Phi'(k_x) = -\frac{\int x W(x,k_x)dx}{\int W(x,k_x)dx}. \quad (4)$$

Therefore, once given the predesigned trajectory $X = f(Z)$, a WDF can be constructed based on Eq. (2) and then the necessary initial field distribution as well as the angular spectrum can be readily figured out using Eqs. (3) and (4). This is the essential idea of our theoretical analysis, which is consistent for both 2D and 3D fields as mentioned. In the following, we apply this approach to some specific cases to demonstrate its wide suitability.

III. DESIGN OF LIGHT BEAMS IN 2D SPACE

First, we discuss the case of 2D fields and mainly consider the caustic of a power-law trajectory $X = f(Z) = a_n Z^n (a_n > 0, n \neq 1)$, which is the case widely investigated with previous caustic methods [27–30] and thus suitable for comparison between our approach and those caustic methods. In this case, the constructed WDF can be figured out based on Eq. (2), which reads

$$W(x,k_x) = \frac{\delta(k_x - na_n k\{-x/[(n-1)a_n]\}^{1-1/n})}{|n(n-1)a_n k\{-x/[(n-1)a_n]\}^{1-1/n}|}. \quad (5)$$

This result shows the relationship between x and k_x in phase space, as shown in Fig. 1(c). After a further calculation based on Eqs. (3) and (4) (see Appendix A), we can obtain the initial field distribution,

$$\rho^2(x) = A_n(-x)^{-1+1/n}, \quad \varphi(x) = B_n(-x)^{2-1/n}, \quad (6)$$

and the angular spectrum,

$$P^2(k_x) = C_n k_x^{1-1/(n-1)}, \quad \Phi(k_x) = D_n k_x^{2+1/(n-1)}. \quad (7)$$

The obtained phase distributions in Eqs. (6) and (7) are consistent with previous caustic methods either in real space [27,28] or in Fourier space [29,30], which shows, on one hand, the reliability of our approach and, on the other hand, the inner connection between the two previous caustic methods from the perspective of the WDF. Apart from this, our analysis also gives the initial amplitude distribution, which relates to the intensity variation along the caustic [39].

Based on the above theoretical results, some accelerating beams propagating along specific trajectories are demonstrated in Fig. 2 based on the numerical calculation of the paraxial angular spectrum integral, and a full-wave analysis has also been carried out to confirm these results as shown in Appendix B. The powers n of the trajectories include 3, 2, and 3/2, with beams shaped in both real space and Fourier
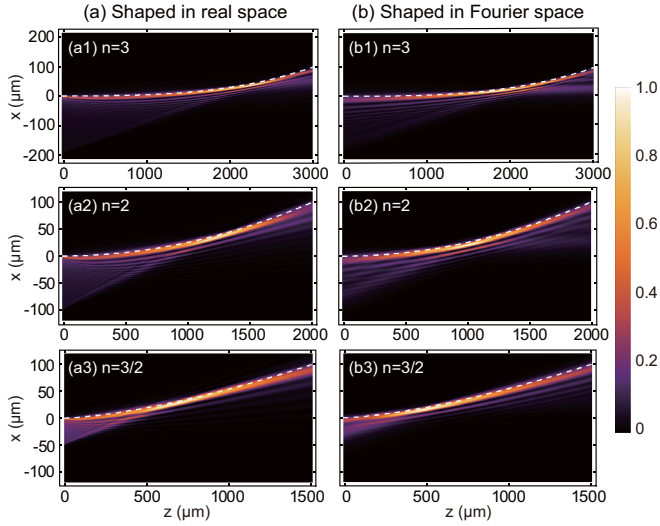
FIG. 2. Intensity distribution of accelerating beams propagating along power-law trajectories with power n chosen to be 3, 2, and 3/2 for demonstration. Accelerating beams are constructed in (a) real space and (b) Fourier space based on the initial field distribution and the angular spectrum, respectively. The predesigned trajectories are depicted by dashed curves.
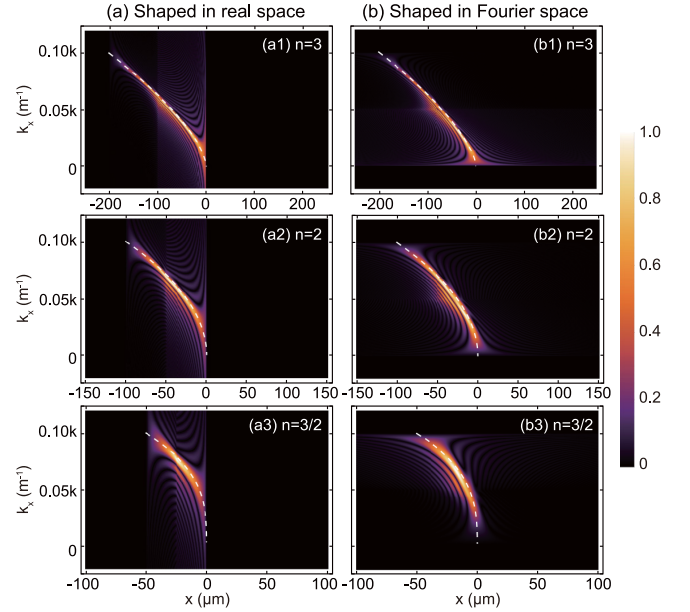

FIG. 3. Comparison between real WDFs and constructed WDFs for the accelerating beams demonstrated in Fig. 2. Real WDFs are calculated based on the definition in Eq. (1) and then normalized and presented as absolute values here, while WDFs constructed according to Eq. (2) are represented by the corresponding dashed curves.

space. As shown clearly, the main lobes of the light beams propagate exactly along the predesigned trajectories, which further confirms the validity of our analysis. Moreover, for the same caustic trajectory, the beams shaped in real space and in Fourier space always behave similarly on the whole. This, on one hand, unifies the previous works' results obtained either in real space or in Fourier space [27–30] and, on the other hand, provides more than one experimental generation scheme for the same caustic trajectory, including light fields shaped in real space, Fourier space (realized by a Fourier lens), and even their combination.

Furthermore, it is natural to wonder why this constructed WDF in phase space is capable of designing accelerating beams properly. To answer this question, the real WDFs in phase space of the above demonstrated accelerating beams obtained by Eq. (1) are shown in Fig. 3, and for comparison, the constructed WDFs are depicted by dashed curves. In fact, they are not identical, which means that actually no light beams exactly correspond to these constructed WDFs. However, as shown in Fig. 3, these constructed WDFs match well with the major part of the real ones, indicating that the constructed WDF is actually a simplified yet effective approximation to the real one when considering only the most significant light rays forming the caustic. Thus the phase-space design of the WDF is a useful and effective approach in designing accelerating beams for specific applications.

IV. DESIGN OF LIGHT BEAMS IN 3D SPACE

It has been shown that the phase-space design of the WDF is a useful tool to tailor accelerating beams along a predesigned trajectory in the 2D plane, which unifies previous caustic methods in real space and Fourier space. In the following, we move to the case of 3D fields, including the situation where the light fields along two transverse directions are inseparable

and thus unable to be separated into the 2D case, beyond the analytical scope of the previous caustic methods. Here we first discuss a general 3D caustic curve in the form of

$$X = f(t + t_0), \quad Y = g(t + t_0), \quad Z = at, \qquad (8)$$

where t is the parameter of this parametric equation, while t_0 and a are undetermined variables. In this case, the constructed WDF can be expressed as

$$W(x,y,k_x,k_y) = \int_0^{t_{\max}} \begin{aligned} &\delta[x - F_1(t,t_0), y - G_1(t,t_0)] \\ &\cdot \delta[k_x - F_2(t,t_0), k_y - G_2(t,t_0)]dt, \end{aligned}$$
$$(9)$$

where the expressions of $F_1(t,t_0)$, $F_2(t,t_0)$, $G_1(t,t_0)$, and $G_2(t,t_0)$ are given in Appendix C. After a further detailed derivation (see Appendix D), it is interesting to arrive at a natural constraint for the trajectory

$$[f'(t + t_0)]^2 + [g'(t + t_0)]^2 = \text{const} \stackrel{\Delta}{=} u^2, \qquad (10)$$

which requires k_r to be a constant, corresponding to the requirement for nondiffracting beams [40]. Note that there is one class of caustic trajectories satisfying the above constraint

$$\begin{aligned} f'(t + t_0) &= -u \sin[h(t + t_0)], \\ g'(t + t_0) &= u \cos[h(t + t_0)], \end{aligned} \qquad (11)$$

where $h(t + t_0)$ is an arbitrary function, and we mainly discuss these trajectories in the following.

Consider the case of $h(t + t_0) = t + t_0$, corresponding to a helical trajectory as shown by the red curve in Fig. 4. Applying the constructed WDF in the same way, we can also obtained
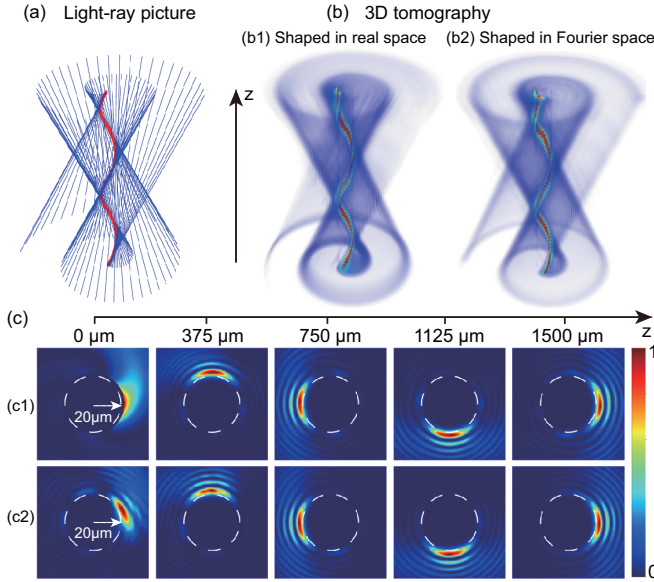
FIG. 4. Simulation results for constructed helical beams. (a) A light-ray picture describing a bundle of light rays (in blue) forming a helical caustic (in red). (b) The 3D tomography showing the propagation dynamics of two-cycle helical beams constructed in (b1) real space and (b2) Fourier space, respectively. (c) Cross-sectional intensity distributions in the first cycle are presented in detail for the above helical beams shaped in (c1) real space and (c2) Fourier space, with the dashed circle of radius 20 μm representing the projection of the helical caustic to the initial plane.
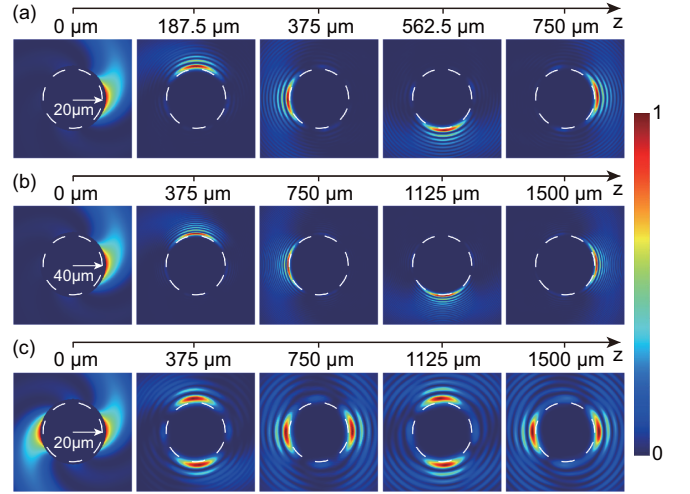

FIG. 5. Cross-sectional intensity distributions of helical beams constructed in real space under different parameters in comparison with Fig. 4(c1). (a) Radius $u = 20$ μm, period $2\pi a = 750$ μm; (b) radius $u = 40$ μm, period $2\pi a = 1500$ μm; (c) radius $u = 20$ μm, period $2\pi a = 1500$ μm, two lobes.

the required initial field distribution

$$\rho^2(r,\theta) = \frac{\delta[\theta - \sqrt{r^2/u^2 - 1} + \arccos(u/r) - t_0]}{\sqrt{r^2 - u^2}}, \quad (12)$$

$$\varphi(r,\theta) = [\theta - \sqrt{r^2/u^2 - 1} + \arccos(u/r)]u^2 k/a$$

and angular spectrum

$$P^2(k_r, k_\theta) = \delta(k_r - uk/a)/k_r$$
$$\Phi(k_r, k_\theta) = uk_r(k_\theta - \pi/2 - t_0) \quad (13)$$

in the polar coordinate.

It is noted that the intensity of the initial field distribution and the angular spectrum are both Dirac functions, which results from the predesigned caustic being a curve rather than a surface in 3D space, as shown in Fig. 4(a). If the caustic curve slightly extends to a surface (e.g., t_0 or a varies within a certain range in this case), the intensity distribution in the form of the Dirac function will be replaced by a finite-width function, and the choice of this width needs to balance the confinement and divergence of the main lobe.

On the other hand, the phase distribution of the angular spectrum is similar to the one directly proposed for helico-conical beams [36,37]. Although it has been observed in those works that the head of the spiral propagates along a helical trajectory around the optical axis, no further explanation is given for this interesting phenomenon. Here we start from our constructed WDF and naturally associate a helical trajectory with such a phase distribution in Fourier space. Moreover, we also give its counterpart constructed in real space, which is

similar to that in Ref. [38]. Here we investigate in the paraxial regime and provide a more clear relation between the helical caustic and the initial spiral-shaped field distribution.

Based on Eqs. (12) and (13), we have designed a two-cycle helical caustic with radius $u = 20$ μm and period $2\pi a = 1500$ μm for demonstration. The simulation results are shown in Fig. 4(b) in the form of 3D tomography to illustrate the propagation dynamics, while the cross-sectional intensity distributions in the first cycle are presented in Fig. 4(c), with the dashed circle representing the projection of the predesigned helical caustic to the initial plane. It is worth mentioning that this constructed helical beam is highly adjustable and customizable, including the radius, the period, the number of periods, and even the number of main lobes as shown in Fig. 5, which provides great flexibility in applications.

Apart from the case of $h(t + t_0) = t + t_0$, corresponding to a helical caustic, there is still a variety of 3D caustics contained in Eq. (10). In the following, we discuss another two cases: $h(t + t_0) = (t + t_0)^{1/2}$ and $h(t + t_0) = (t + t_0)^2$. The accelerating beams are constructed in Fourier space and their propagation dynamics are presented in Figs. 6(a) and 6(b). The dashed curve in the cross-sectional intensity distribution is the projection of the predesigned caustic to the initial plane, which is an involute of circle for the case of $h(t + t_0) = (t + t_0)^{1/2}$ and a Cornu spiral for $h(t + t_0) = (t + t_0)^2$. As shown in Fig. 6(a) and 6(b), the main lobe of each beam propagates exactly along the predesigned trajectory and is well confined in it. When it comes to the end of the trajectory, the main lobe starts to spread out as expected. In addition, the direction of these beams' rotation can also be reversed, corresponding to the cases of $h(t + t_0) = -(t + t_0)^{1/2}$ and $h(t + t_0) = -(t + t_0)^2$ as shown in Figs. 6(c) and 6(d). These results further confirm the existence of a wide-ranging class of 3D accelerating beams contained in Eq. (10).

Before closing, we would like to point out that the proposed method of constructing accelerating beams by designing the WDF is not limited to the paraxial situation, and the case
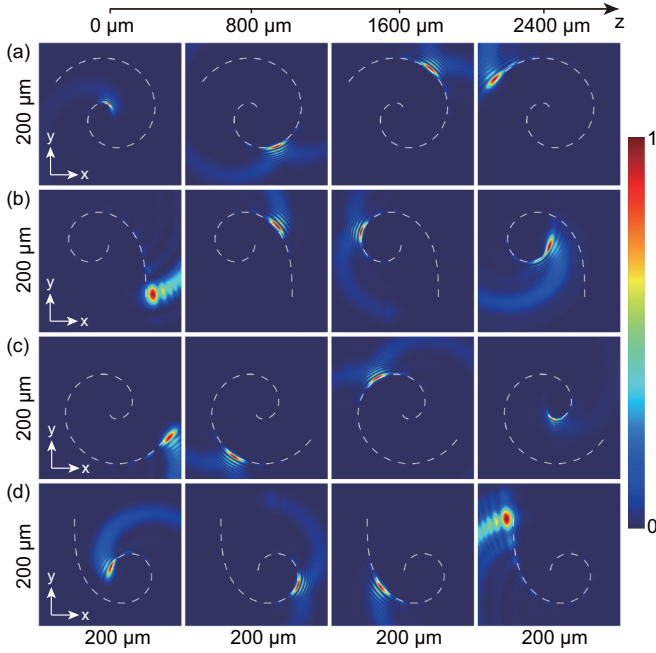
FIG. 6. Simulating propagation dynamics for the case of (a) $h(t + t_0) = (t + t_0)^{1/2}$ and (b) $h(t + t_0) = (t + t_0)^2$. The cross-sectional intensity distribution during propagation is presented for accelerating beams constructed in Fourier space and the dashed curve in it is (a) an involute of circle and (b) a Cornu spiral, representing the projection of the predesigned caustic into the initial plane.

discussed above is used for its relatively simple results to better illustrate the idea of WDF-based design. Extension to the nonparaxial situation can be achieved by a slight modification to the definition of the constructed WDF in Eq. (2), and some nonparaxial cases such as circular beams as shown in Fig. 8 (Appendix E) have been constructed successfully based on this method. Since the real WDF of the light field has a more general definition in the nonparaxial regime [33], it is expected to have more to be explored in this regime compared with the above discussion in the future work.

V. CONCLUSION

In conclusion, we propose a new approach to the construction of accelerating beams by designing the WDF in phase space. Based on the constructed WDF, we can readily obtain the necessary initial field distribution in real space and angular spectrum in Fourier space simultaneously. To show its widespread suitability, first in the 2D case, we analyze accelerating beams moving along power-law trajectories, which unifies previous caustic methods proposed in real space and Fourier space; later, in the 3D case, we reveal a new class of 3D accelerating beams including the familiar helical beam, beyond the analytical scope of previous caustic methods. The phase-space design of accelerating beams put forward here is intuitive, widely applicable, and easy to handle; it is expected to find important applications in the demand for highly tailored accelerating beams, ranging from particle manipulation to material processing. It also deepens our understanding of accelerating beams from a new perspective

and may further advance the field of engineering wave fronts for future applications.

APPENDIX A: DERIVATIONS OF EQS. (6) AND (7) IN THE CASE OF 2D SPACE

Based on Eqs. (3) and (4) as well as the given WDF in Eq. (5), we can calculate the initial field distribution,

$$
\begin{aligned}
\rho^2(x) &= \int W(x, k_x) dk_x \\
&= \int \frac{\delta(k_x - n a_n k \{-x/[(n-1)a_n]\}^{1-1/n})}{n(n-1)a_n k \{-x/[(n-1)a_n]\}^{1-1/n}} dk_x \\
&= (n(n-1)a_n k \{-x/[(n-1)a_n]\}^{1-1/n})^{-1} \\
&= k^{-1} n^{-1} [(n-1)a_n]^{-1/n} (-x)^{-1+1/n} \\
&\triangleq A_n (-x)^{-1+1/n},
\end{aligned} \tag{A1}
$$

$$
\begin{aligned}
\varphi'(x) &= \frac{\int k_x W(x, k_x) dk_x}{\int W(x, k_x) dk_x} \\
&= \frac{\int k_x \delta(k_x - n a_n k \{-x/[(n-1)a_n]\}^{1-1/n}) dk_x}{\int \delta(k_x - n a_n k \{-x/[(n-1)a_n]\}^{1-1/n}) dk_x} \\
&= n a_n k \{-x[(n-1)a_n]\}^{1-1/n} \\
&= k n (n-1)^{1/n-1} a_n^{1/n} (-x)^{1-1/n},
\end{aligned} \tag{A2}
$$

$$
\begin{aligned}
\varphi(x) &= -k n^2 (n-1)^{1/n-1} (2n-1)^{-1} a_n^{1/n} (-x)^{2-1/n} \\
&\triangleq B_n (-x)^{2-1/n},
\end{aligned} \tag{A3}
$$

as well as the angular spectrum,

$$
\begin{aligned}
P^2(k_x) &= \int W(x, k_x) dx \\
&= \int \frac{\delta(k_x - n a_n k \{-x/[(n-1)a_n]\}^{1-1/n})}{n(n-1)a_n k \{-x/[(n-1)a_n]\}^{1-1/n}} dx \\
&= \{n(n-1)a_n [k_x/(n a_n k)]^{1-1/(n-1)}\}^{-1} \\
&= k^{1/(n-1)-1}(n-1)(n a_n)^{1/(n-1)} k_x^{1-1/(n-1)} \\
&\triangleq C_n k_x^{1-1/(n-1)},
\end{aligned} \tag{A4}
$$

$$
\begin{aligned}
\Phi'(k_x) &= -\frac{\int x W(x, k_x) dx}{\int W(x, k_x) dx} \\
&= -\frac{\int x \delta\{x + (n-1)a_n [k_x/(n a_n k)]^{1+1/(n-1)}\} dx}{\int \delta\{x + (n-1)a_n [k_x/(n a_n k)]^{1+1/(n-1)}\} dx} \\
&= (n-1)a_n [k_x/(n a_n k)]^{1+1/(n-1)} \\
&= (kn)^{-1-1/(n-1)}(n-1) a_n^{-1/(n-1)} k_x^{1+1/(n-1)},
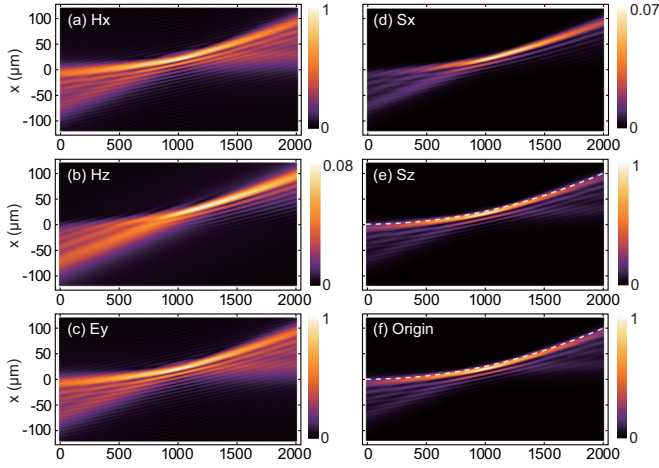\end{aligned} \tag{A5}
$$

FIG. 7. Comparison of results obtained by (a)–(e) full-wave analysis and (f) paraxial-wave approximation. Specifically, the results show amplitude distributions of field components of (a) H_x, (b) H_z, and (c) E_y and Poynting components of (d) S_x and (e) S_z, compared with (f) the optical intensity distribution in Fig. 2(b2). Note that the magnetic field and Poynting vector are normalized to H_x and S_z, respectively, and the predesigned trajectory is shown by the dashed curve.

$$\Phi(k_x) = (kn)^{-1-1/(n-1)}(n-1)^2(2n-1)^{-1}a_n^{-1/(n-1)}k_x^{2+1/(n-1)}$$
$$\stackrel{\triangle}{=} D_n k_x^{2+1/(n-1)}. \qquad (A6)$$

APPENDIX B: FULL-WAVE ANALYSIS

Here we carry out the full-wave analysis for the TE-polarized wave in our 2D case based on the diffraction integral. More specifically, the component E_y is first worked out by calculating the nonparaxial angular-spectrum integral with the initial angular spectrum as designed previously, and then the other components, H_x and H_z, as well as the Poynting components, S_x and S_z, can be obtained based on Eq. (B1). For illustration, we perform this calculation for the case of a power-law trajectory with $n = 2$ designed in Fourier space, corresponding to Fig. 2(b2). The results obtained in this case are shown in Figs. 7(a)–7(e), in comparison with the original result in Fig. 7(f), the same as Fig. 2(b2) in the text. As can be seen, the Poynting component S_z is dominating and matches well with the original result. To have quantifiable values for this comparison, we have calculated the overlap integral between Fig. 7(e) and Fig. 7(f), which is defined as Eq. (B2), where $S_1(x,z)$ and $S_2(x,z)$ are the two compared distribution functions. The correlation is calculated to be as high as 99.4% in this case, and 95.3% and 99.6% in the other two cases, $n = 3$ and $n = 3/2$, respectively, which confirms the accuracy of our simulation under the scalar and paraxial wave analysis in the text:

$$H_x = -\frac{1}{j\omega\mu_0}\frac{\partial E_y}{\partial z}, \quad H_z = \frac{1}{j\omega\mu_0}\frac{\partial E_y}{\partial x},$$
$$S_x = E_y H_z, \quad S_z = -E_y H_x, \qquad (B1)$$

$$\text{Cor} = \frac{\iint S_1(x,z)S_2(x,z)dxdz}{\sqrt{\iint S_1^2(x,z)dxdz \iint S_2^2(x,z)dxdz}}. \qquad (B2)$$

APPENDIX C: EXPRESSIONS FOR SOME SYMBOLS

$$F_1(t,t_0) = f(t+t_0) - tf'(t+t_0), \qquad (C1)$$

$$F_2(t,t_0) = ka^{-1}f'(t+t_0), \qquad (C2)$$

$$G_1(t,t_0) = g(t+t_0) - tg'(t+t_0), \qquad (C3)$$

$$G_2(t,t_0) = ka^{-1}g'(t+t_0). \qquad (C4)$$

APPENDIX D: DERIVATIONS OF EQ. (10), A NATURAL CONSTRAINT IN THE CASE OF 3D SPACE

First, considering the real space, based on Eq. (9), we can calculate the initial field distribution including the intensity distribution,

$$\rho^2(x,y) = \iint W(x,y,k_x,k_y)dk_xdk_y$$
$$= \int_0^{t_{\max}} \delta[x - F_1(t,t_0), y - G_1(t,t_0)]dt, \qquad (D1)$$

and the derivatives of the phase distribution with respect to the space coordinates x and y,

$$\frac{\partial\varphi(x,y)}{\partial x} = \frac{\iint k_x W(x,y,k_x,k_y)dk_xdk_y}{\iint W(x,y,k_x,k_y)dk_xdk_y}$$
$$= \frac{\int_0^{t_{\max}} F_2(t,t_0)\delta[x - F_1(t,t_0), y - G_1(t,t_0)]dt}{\int_0^{t_{\max}} \delta[x - F_1(t,t_0), y - G_1(t,t_0)]dt}$$
$$= F_2(t,t_0)|_{t=F_1^{-1}(x,t_0)}, \qquad (D2)$$

$$\frac{\partial\varphi(x,y)}{\partial y} = G_2(t,t_0)|_{t=G_1^{-1}(x,t_0)}. \qquad (D3)$$

Since the relations of the variables x and y and the variables t and t_0 are

$$x = F_1(t,t_0) = f(t+t_0) - tf'(t+t_0), \qquad (D4)$$

$$y = G_1(t,t_0) = g(t+t_0) - tg'(t+t_0), \qquad (D5)$$

the derivatives of the phase distribution with respect to the variables t and t_0 can be obtained by applying the chain rule,

$$\frac{\partial\varphi(x,y)}{\partial t} = \frac{\partial\varphi}{\partial x}\cdot\frac{\partial x}{\partial t} + \frac{\partial\varphi}{\partial y}\cdot\frac{\partial y}{\partial t}$$
$$= -ka^{-1}t[f'(t+t_0)f''(t+t_0)$$
$$+ g'(t+t_0)g''(t+t_0)], \qquad (D6)$$

$$\frac{\partial\varphi(x,y)}{\partial t_0} = \frac{\partial\varphi}{\partial x}\cdot\frac{\partial x}{\partial t_0} + \frac{\partial\varphi}{\partial y}\cdot\frac{\partial y}{\partial t_0}$$
$$= ka^{-1}\{[f'(t+t_0)]^2 + [g'(t+t_0)]^2$$
$$- t[f'(t+t_0)f''(t+t_0) + g'(t+t_0)g''(t+t_0)]\}. \qquad (D7)$$

Furthermore, the mixed second derivatives can be obtained:

$$\frac{\partial^2\varphi(x,y)}{\partial t\partial t_0} = -ka^{-1}t\{[f''(t+t_0)]^2 + f'(t+t_0)f'''(t+t_0)$$
$$+ [g''(t+t_0)]^2 + g'(t+t_0)g'''(t+t_0)\}, \qquad (D8)$$

$$\frac{\partial^2 \varphi(x,y)}{\partial t_0 \partial t} = -ka^{-1}t\{[f''(t+t_0)]^2 + f'(t+t_0)f'''(t+t_0)$$
$$+ [g''(t+t_0)]^2 + g'(t+t_0)g'''(t+t_0)\}$$
$$+ ka^{-1}[f'(t+t_0)f''(t+t_0)$$
$$+ g'(t+t_0)g''(t+t_0)]. \quad \text{(D9)}$$

For a continuous function, these mixed second derivatives are equal, which leads to a constraint of

$$f'(t+t_0)f''(t+t_0) + g'(t+t_0)g''(t+t_0) = 0 \quad \text{(D10)}$$

and can be further written as

$$[f'(t+t_0)]^2 + [g'(t+t_0)]^2 = \text{const} \equiv u^2. \quad \text{(D11)}$$

This is the constraint presented in Eq. (10). Moreover, bringing this condition back to Eqs. (D6) and (D7) can derive the corresponding phase distribution,

$$\frac{\partial \varphi(x,y)}{\partial t} = 0, \quad \frac{\partial \varphi(x,y)}{\partial t_0} = u^2 ka^{-1} \Rightarrow \varphi(x,y) = u^2 ka^{-1} t_0. \quad \text{(D12)}$$

Similarly, considering the Fourier space, we can obtain the angular spectrum including the intensity distribution,

$$P^2(k_x,k_y) = \iint W(x,y,k_x,k_y)dxdy$$
$$= \int_0^{t_{\max}} \delta[k_x - F_2(t,t_0), k_y - G_2(t,t_0)]dt, \quad \text{(D13)}$$

and the derivatives of the phase distribution with respect to the spatial frequency k_x and k_y,

$$\frac{\partial \Phi(k_x,k_y)}{\partial k_x} = -\frac{\iint x W(x,y,k_x,k_y)dxdy}{\iint W(x,y,k_x,k_y)dxdy}$$
$$= -F_1(t,t_0)|_{t=F_2^{-1}(x,t_0)}, \quad \text{(D14)}$$

$$\frac{\partial \Phi(k_x,k_y)}{\partial k_y} = -G_1(t,t_0)|_{t=G_2^{-1}(x,t_0)}. \quad \text{(D15)}$$

Since the relations of variables k_x and k_y and variables t and a are

$$k_x = F_2(t,t_0) = ka^{-1}f'(t+t_0), \quad \text{(D16)}$$

$$k_y = G_2(t,t_0) = ka^{-1}g'(t+t_0), \quad \text{(D17)}$$

the derivatives of the phase distribution with respect to variables t and a can be obtained by applying the chain
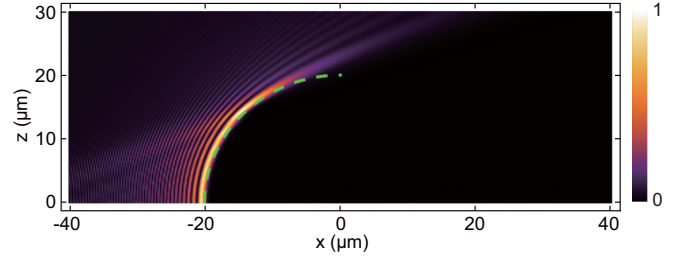

FIG. 8. Intensity distribution of a circular beam constructed in the nonparaxial regime with our proposed method. The dashed curve represents the designed circle of radius 20 μm.

rule:

$$\frac{\partial \Phi(k_x,k_y)}{\partial t} = \frac{\partial \Phi}{\partial k_x} \cdot \frac{\partial k_x}{\partial t} + \frac{\partial \Phi}{\partial k_y} \cdot \frac{\partial k_y}{\partial t}$$
$$= -[f(t+t_0) - tf'(t+t_0)] \cdot ka^{-1}f''(t+t_0)$$
$$- [g(t+t_0) - tg'(t+t_0)] \cdot ka^{-1}g''(t+t_0), \quad \text{(D18)}$$

$$\frac{\partial \Phi(k_x,k_y)}{\partial a} = \frac{\partial \Phi}{\partial k_x} \cdot \frac{\partial k_x}{\partial a} + \frac{\partial \Phi}{\partial k_y} \cdot \frac{\partial k_y}{\partial a}$$
$$= [f(t+t_0) - tf'(t+t_0)] \cdot ka^{-2}f'(t+t_0)$$
$$+ [g(t+t_0) - tg'(t+t_0)] \cdot ka^{-2}g'(t+t_0). \quad \text{(D19)}$$

Furthermore, the mixed second derivatives can be obtained:

$$\frac{\partial^2 \Phi(k_x,k_y)}{\partial t \partial a} = [f(t+t_0) - tf'(t+t_0)] \cdot ka^{-2}f''(t+t_0)$$
$$+ [g(t+t_0) - tg'(t+t_0)] \cdot ka^{-2}g''(t+t_0), \quad \text{(D20)}$$

$$\frac{\partial^2 \Phi(k_x,k_y)}{\partial a \partial t} = [f(t+t_0) - tf'(t+t_0)] \cdot ka^{-2}f''(t+t_0)$$
$$+ [g(t+t_0) - tg'(t+t_0)] \cdot ka^{-2}g''(t+t_0)$$
$$- ka^{-2}t[f'(t+t_0)f''(t+t_0)$$
$$+ g'(t+t_0)g''(t+t_0)]. \quad \text{(D21)}$$

The equality of these mixed second derivatives also leads to the same constraint as in Eq. (D11). Bringing this condition back to Eqs. (D18) and (D19) we can also obtain the corresponding phase distribution,

$$\Phi(k_x,k_y) = ka^{-1}[u^2 t - f(t+t_0)f'(t+t_0)$$
$$- g(t+t_0)g'(t+t_0)]. \quad \text{(D22)}$$

APPENDIX E: EXTENSION TO THE NONPARAXIAL CASE

Extension to the nonparaxial case is illustrated in Fig. 8.

[1] J. K. Gansel, M. Thiel, M. S. Rill, M. Decker, K. Bade, V. Saile, G. von Freymann, S. Linden, and M. Wegener, Science **325**, 1513 (2009).

[2] N. Yu, P. Genevet, M. A. Kats, F. Aieta, J.-P. Tetienne, F. Capasso, and Z. Gaburro, Science **334**, 333 (2011).

[3] D. Lin, P. Fan, E. Hasman, and M. L. Brongersma, Science **345**, 298 (2014).

[4] I. Dolev, I. Epstein, and A. Arie, Phys. Rev. Lett. **109**, 203903 (2012).

[5] E. Maguid, I. Yulevich, D. Veksler, V. Kleiner, M. L. Brongersma, and E. Hasman, Science **352**, 1202 (2016).

[6] N. Yu and F. Capasso, Nat. Mater. **13**, 139 (2014).

[7] G. A. Siviloglou and D. N. Christodoulides, Opt. Lett. **32**, 979 (2007).

[8] G. A. Siviloglou, J. Broky, A. Dogariu, and D. N. Christodoulides, Phys. Rev. Lett. **99**, 213901 (2007).

[9] J. Baumgartl, M. Mazilu, and K. Dholakia, Nat. Photon. **2**, 675 (2008).

[10] J. Zhao, I. D. Chremmos, D. Song, D. N. Christodoulides, N. K. Efremidis, and Z. Chen, Sci. Rep. **5**, 12086 (2015).

[11] A. Mathis, F. Courvoisier, L. Froehly, L. Furfaro, M. Jacquot, P. A. Lacourt, and J. M. Dudley, Appl. Phys. Lett. **101**, 071110 (2012).

[12] S. Jia, J. C. Vaughan, and X. Zhuang, Nat. Photon. **8**, 302 (2014).

[13] T. Vettenburg, H. I. C. Dalgarno, J. Nylk, C. Coll-Lladó, D. E. K. Ferrier, T. Čižmár, F. J. Gunn-Moore, and K. Dholakia, Nat. Method **11**, 541 (2014).

[14] P. Rose, F. Diebel, M. Boguslawski, and C. Denz, Appl. Phys. Lett. **102**, 101101 (2013).

[15] A. Chong, W. H. Renninger, D. N. Christodoulides, and F. W. Wise, Nat. Photon. **4**, 103 (2010).

[16] D. Abdollahpour, S. Suntsov, D. G. Papazoglou, and S. Tzortzakis, Phys. Rev. Lett. **105**, 253901 (2010).

[17] M. Clerici, Y. Hu, P. Lassonde, C. Milián, A. Couairon, D. N. Christodoulides, Z. Chen, L. Razzari, F. Vidal, F. Légaré, D. Faccio, and R. Morandotti, Sci. Adv. **1**, e1400111 (2015).

[18] P. Polynkin, M. Kolesik, J. V. Moloney, G. A. Siviloglou, and D. N. Christodoulides, Science **324**, 229 (2009).

[19] P. Zhang, T. Li, J. Zhu, X. Zhu, S. Yang, Y. Wang, X. Yin, and X. Zhang, Nat. Commun. **5**, 4316 (2014).

[20] N. Voloch-Bloch, Y. Lereah, Y. Lilach, A. Gover, and A. Arie, Nature **494**, 331 (2013).

[21] A. Minovich, A. E. Klein, N. Janunts, T. Pertsch, D. N. Neshev, and Y. S. Kivshar, Phys. Rev. Lett. **107**, 116802 (2011).

[22] L. Li, T. Li, S. M. Wang, C. Zhang, and S. N. Zhu, Phys. Rev. Lett. **107**, 126804 (2011).

[23] I. Epstein and A. Arie, Phys. Rev. Lett. **112**, 023903 (2014).

[24] M. Berry and C. Upstill, in *Progress in Optics XVIII* (Elsevier, Amsterdam, 1980), pp. 257–346.

[25] Y. A. Kravtsov and Y. I. Orlov, Sov. Phys. Usp. **26**, 1038 (1983).

[26] P. Vaveliuk, A. Lencina, J. A. Rodrigo, and O. M. Matos, Phys. Rev. A **92**, 033850 (2015).

[27] E. Greenfield, M. Segev, W. Walasik, and O. Raz, Phys. Rev. Lett. **106**, 213902 (2011).

[28] L. Froehly, F. Courvoisier, A. Mathis, M. Jacquot, L. Furfaro, R. Giust, P. A. Lacourt, and J. M. Dudley, Opt. Express **19**, 16455 (2011).

[29] Y. Hu, D. Bongiovanni, Z. Chen, and R. Morandotti, Phys. Rev. A **88**, 043809 (2013).

[30] D. Bongiovanni, Y. Hu, B. Wetzel, R. A. Robles, G. G. Mendoza, E. A. Martipanameo, Z. Chen, and R. Morandotti, Sci. Rep. **5**, 13197 (2015).

[31] Y. Wen, Y. Chen, Y. Zhang, H. Chen, and S. Yu, Phys. Rev. A **94**, 013829 (2016).

[32] R.-P. Chen, H.-P. Zheng, and C.-Q. Dai, J. Opt. Soc. Am. A **28**, 1307 (2011).

[33] M. A. Alonso, Adv. Opt. Photon. **3**, 272 (2011).

[34] M. J. Bastiaans, J. Opt. Soc. Am. **69**, 1710 (1979).

[35] L. Waller, G. Situ, and J. W. Fleischer, Nat. Photon. **6**, 474 (2012).

[36] C. A. Alonzo, P. J. Rodrigo, and J. Glückstad, Opt. Express **13**, 1749 (2005).

[37] V. R. Daria, D. Z. Palima, and J. Glückstad, Opt. Express **19**, 476 (2011).

[38] H. Liu, M. Q. Mehmood, K. Huang, L. Ke, H. Ye, P. Genevet, M. Zhang, A. Danner, S. P. Yeo, C.-W. Qiu, and J. Teng, Adv. Opt. Mater. **2**, 1193 (2014).

[39] R. Schley, I. Kaminer, E. Greenfield, R. Bekenstein, Y. Lumer, and M. Segev, Nat. Commun. **5**, 5189 (2014).

[40] S. López-Aguayo, Y. V. Kartashov, V. A. Vysloukh, and L. Torner, Phys. Rev. Lett. **105**, 013902 (2010).